

## **REGULAR PAPER • OPEN ACCESS**

# The polarization field in Al-rich AlGaN multiple quantum wells

To cite this article: Qiang Guo et al 2019 Jpn. J. Appl. Phys. 58 SCCC10

View the <u>article online</u> for updates and enhancements.

https://doi.org/10.7567/1347-4065/ab07a9



# The polarization field in Al-rich AlGaN multiple quantum wells

Qiang Guo<sup>1\*</sup>, Ronny Kirste<sup>1,2</sup>, Seiji Mita<sup>1,2</sup>, James Tweedie<sup>1,2</sup>, Pramod Reddy<sup>1,2</sup>, Shun Washiyama<sup>1</sup>, M. Hayden Breckenridge<sup>1</sup>, Ramón Collazo<sup>1</sup>, and Zlatko Sitar<sup>1,2</sup>

<sup>1</sup>Department of Materials Science and Engineering, North Carolina State University, Raleigh, NC 27695, United States of America

Received December 19, 2018; revised January 22, 2019; accepted January 23, 2019; published online May 9, 2019

This paper investigates the quantum confined Stark effect in AlGaN multiple quantum well structures with a high Al content grown on single-crystalline AlN substrates. The quantitative relationship between the quantum well structure parameters, photogenerated carrier density, built-in electric field and ground-level emission is discussed. It is found that the electric field strength increases from  $0.5 \, \text{MV cm}^{-1}$  to almost  $3 \, \text{MV cm}^{-1}$  when the Al content in the quantum well barriers is increased from 65% to 100%, which is consistent with the theory of spontaneous and piezoelectric polarization in III-nitrides. In addition, the built-in electric field increases significantly with increasing barrier thickness. Based on these results, the electric field in an  $Al_{0.55}Ga_{0.45}N$  single quantum well with AlN cladding is predicted to be around  $5 \, \text{MV cm}^{-1}$ .

### 1. Introduction

AlGaN-based optoelectronic devices are predicted to have a broad range of mid-ultraviolet (200–300 nm) applications, such as water purification, bio-sensing, and covert non-lineof-sight communications. 1-9) To achieve sufficient device performance, a high internal quantum efficiency (IQE) in the active region is needed. 4,10,11) However, recent studies 4,12–14) showed that the quantum confined Stark effect (QCSE) significantly affects the IQE. For AlGaN quantum wells (QWs) grown along the c-direction, the QCSE cannot be ignored due to a strong polarization-related built-in electric field. In the presence of this electric field, electrons and holes are pushed in the opposite directions, causing a reduction in the overlap between the electron and hole wavefunctions and a significant decrease in the IQE of QWs. 4,12,13) To mitigate this effect, a very thin well width (2-3 nm) is typically used in current AlGaN multiple quantum well (MQW) designs. This gives rise to better carrier confinement and effectively improves the overlap of electron and hole wavefunctions.

The origin of the built-in electric field in III-nitrides has been widely discussed over the years and is generally thought to be a consequence of both spontaneous polarization (SP) and piezoelectric polarization (PZ). SP originates from the intrinsic asymmetry of the bonds in the equilibrium III-nitride wurtzite crystal structure,  $^{15,19}$ ) leading to a polarization field along the c-axis. Strain due to lattice mismatch leads to PZ, which adds to the total polarization vector. PZ is negative for tensile strain and positive for compressive strain, which makes analysis of the total polarization field even more complex. However, recent theoretical studies have indicated that SP represents the main contribution to the electric fields in AlGaN alloy systems.  $^{17}$ 

So far, most of the work on III-nitrides has been done on GaN or InGaN MQWs. <sup>16,18,19,21-29)</sup> Self-consistent models and analytical approaches are typically used to quantitatively describe the QCSE and its influence on ground-level transition. Recently, Ref. 24 derived an analytical model based on perturbation theory to address these QW transitions. It was

shown that the ground-level transitions were dependent on the electric field strength, carrier density and structural parameters of the QW. Furthermore, they explained the peak energy shift in InGaN MQW LEDs under the influence of p–n junction and polarization fields. However, very few studies have addressed this issue in Al-rich AlGaN MQWs. Reference 14 found that the built-in electric field in *c*-plane Al<sub>0.8</sub>Ga<sub>0.2</sub>N/AlN (*x* nm/20 nm) QWs was 2.3 MV cm<sup>-1</sup>. By contrast, Refs. 30 and 31 showed that the electric fields were 0.4–0.5 MV cm<sup>-1</sup> in 10× Al<sub>0.35</sub>Ga<sub>0.65</sub>N/Al<sub>0.49</sub>Ga<sub>0.51</sub>N (*x* nm/1.5 nm) MQWs and 0.9 MV cm<sup>-1</sup> in 11× Al<sub>0.8</sub>Ga<sub>0.2</sub>N/AlN (*x* nm/6 nm) MQW structures, respectively. Therefore, a comprehensive study needs to be carried out in order to clarify this discrepancy and determine the actual electric field present in AlGaN heterostructures.

In this work, we investigate the QCSE in AlGaN MQWs with a high Al content grown on single-crystalline AlN substrates. An analytical model is presented to evaluate the built-in electric field strength in AlGaN MQWs. We discuss the interplay between the QW structure parameters, photoinjected carrier density, built-in electric field, and ground-level emission and show that the electric field strength increases with increasing Al content of the barriers. Additionally, we examine the influence of barrier thickness on the electric field. Results from this work provide a pathway to improve the understanding of built-in electric fields and their influence on the performance of III-nitride optoelectronic devices.

## 2. Experimental methods

AlGaN MQW structures with a high Al content were grown along the (0001) direction of AlN single-crystal substrates with a dislocation density of  $<10^3\,\mathrm{cm}^{-2}$  via low-pressure metalorganic chemical vapor deposition (LP-MOCVD). Trimethylaluminum (TMA), triethylgallium (TEG) and ammonia (NH $_3$ ) were used as sources for Al, Ga and N, respectively. Details on the growth process and AlN substrate preparation can be found elsewhere. Two sets of MQW samples were prepared with various barrier heights (Al content) and barrier thicknesses. The samples were grown



<sup>&</sup>lt;sup>2</sup>Adroit Materials, 2054 Kildaire Farm Rd, Suite 205, Cary, NC 27518, United States of America

<sup>\*</sup>E-mail: qquo4@ncsu.edu

following the same general structure: a 150-nm-thick Al<sub>0.65</sub>Ga<sub>0.35</sub>N waveguide was grown on bulk AlN, followed by the growth of five periods of Al<sub>0.55</sub>Ga<sub>0.45</sub>N MQW, capped with 4 nm AlN. It is worth noting that although the AlN capping layer will induce significant band bending in the AlGaN MQW structure, we did not observe any significant peak shift change between the AlN cap and Al<sub>0.65</sub>Ga<sub>0.35</sub>N cap samples. In the first set of samples, the MQWs had a fixed well width of 3 nm and 4 nm thick barriers, while the Al composition in the barriers was varied from 65%, 75%, 85% to 100% Al. In the second set, four Al<sub>0.55</sub>Ga<sub>0.45</sub>N/AlN  $5\times MQW$  samples were grown with barrier thickness  $L_b$ = 0.5, 1, 2, 4 nm. High-resolution cross-section transmission electron microscopy imaging was conducted to confirm the well width, and barrier thickness. The strain condition of the MQWs was examined by asymmetric (105) reciprocal space mapping (RSM) measurement via X-ray diffraction. The results indicated that the AlGaN layers were pseudomorphically grown on the AlN substrates. Thus, the whole structure was compressively strained and retained the same in-plane lattice constant as the bulk AlN. 7,34,35)

Photoluminescence (PL) measurements were performed at room temperature (297 K) using a pulsed ArF excimer laser ( $\lambda = 193$  nm) with a pulse duration of 10 ns and repetition rate of 100 Hz. The PL spectrum was recorded by a Princeton Instruments Acton SP2750 0.75 m monochromator with a 150 grooves/mm grating, and a PIXIS: 2KBUV cooled charge-coupled device camera via an optical fiber. Details on the experimental setup can be found elsewhere. Action of the excitation power density.

#### 3. Results and discussion

The QCSE is induced by the large built-in electric fields present in AlGaN QWs due to SP and PZ. Experimentally, PL provides the opportunity to investigate the built-in electric fields in QW structures because the emission wavelength will depend on the field strength inducing the QCSE. Time-resolved PL measurement shows that recombination lifetime in the AlGaN MQW is  $\sim$ 300 ps, which indicates that the equilibrium state is reached during the laser pulse. Thus, we can assume that the carrier density has a constant value during the pulse. Figure 1 shows PL spectra of Al<sub>0.55</sub>Ga<sub>0.45</sub>N/AlN MQWs with 3 nm wide wells and 4 nm wide AlN barriers as a function of the excitation power density. It is found that an increase in the excitation power density leads to a blue shift of the emission wavelength (increase in energy). This blue shift in the peak position is due to carrier screening. With increasing excitation power density, a significant number of electron-hole pairs are generated, which leads to the screening of the built-in electric field and a reduction of the QCSE. Under a high excitation power density  $(95 \text{ kW cm}^{-2}, \text{ corresponds to } n = 10^{12} \text{ cm}^{-2} \text{ in Fig. 2}), \text{ the }$ built-in electric field was completely screened and QW emission shifted to a higher energy compared with the lowpower case (8 kW cm<sup>-2</sup>).

The shift of the ground-level transition energy induced by the electric field can be estimated using an analytical model based on perturbation theory:<sup>24)</sup>

$$\Delta E = -\frac{512(m_{\rm e} + m_{\rm h})e^2 F^2 d^4}{243\pi^6 \hbar^2 \chi^2} \tag{1}$$

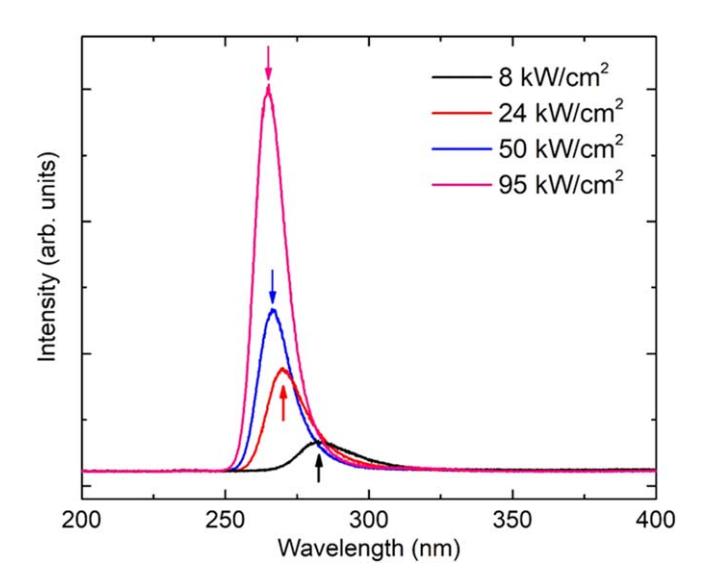


**Fig. 1.** (Color online) Power-dependent PL spectra for an Al<sub>0.55</sub>Ga<sub>0.45</sub>N/AlN MQW with 3 nm/4 nm well/barrier width at room temperature (297 K). An increase in the excitation power density leads to a blue shift of the emission wavelength (increase in energy).

where e is the elementary charge, F is the field strength, d is the well width and  $m_{\rm e}$  and  $m_{\rm h}$  are, respectively, the electron and hole carrier mass. The values of  $m_{\rm e} \sim 0.3 m_0$  and  $m_{\rm h} \sim 2.5 m_0 (m_0 = 9.11 \times 10^{-31} \, {\rm kg})$  for Al<sub>0.55</sub>Ga<sub>0.45</sub>N are estimated based on a linear change in the effective mass with Al content.  $\chi$  describes the electric field screening by the carriers in the QW as given by  $\chi = 1 + n/n_{\rm scr}$ , where

$$n_{\rm scr} = \frac{27\pi^3 \varepsilon_{\rm r} \varepsilon_0 \hbar^2}{80e^2 d^3 (m_{\rm e} + m_{\rm h})} \tag{2}$$

is a screening coefficient in cm<sup>-2</sup> dependent only on the well width, d.  $\varepsilon_0$  and  $\varepsilon_r$  are, respectively, the vacuum permittivity and the relative permittivity of the  $Al_{0.55}Ga_{0.45}N$  well. From this, n is the two-dimensional (2D) concentration of the electron–hole pairs providing suppression of the Stark shift. These two equations directly connect the electric field and the emission energy shift, allowing for an estimation of the built-in field. It should be noted that the perturbation theory is valid under low electric field conditions. In general, III-nitride heterostructures introduce a polarization field on the order of MV cm<sup>-1</sup>, making this analysis appropriate for electrons but close to the applicability limit for holes due to their large effective mass.

First, we investigate the influence of barrier height on the built-in electric field at a constant well and barrier width. Figure 2 shows the relative peak energy shift for MQW structures with different Al contents in the barriers (65%-100%) as a function of the sheet carrier concentration. The sheet carrier concentration is determined with the powerdependent PL using the ABC model. Details on the calculation of the 2D carrier concentration can be found elsewhere. <sup>4,10,37)</sup> As shown in Fig. 2, all PL peaks blue shift with increasing power density. However, the structures with a higher Al content in the barriers show a significantly larger shift than those with a lower Al content. This suggests a stronger Stark shift for the samples with Al-rich barriers due to a higher electric field. Samples with a lower Al content in the barriers have a lower field and, thus, the effect of increasing excitation power density upon the energy shift is

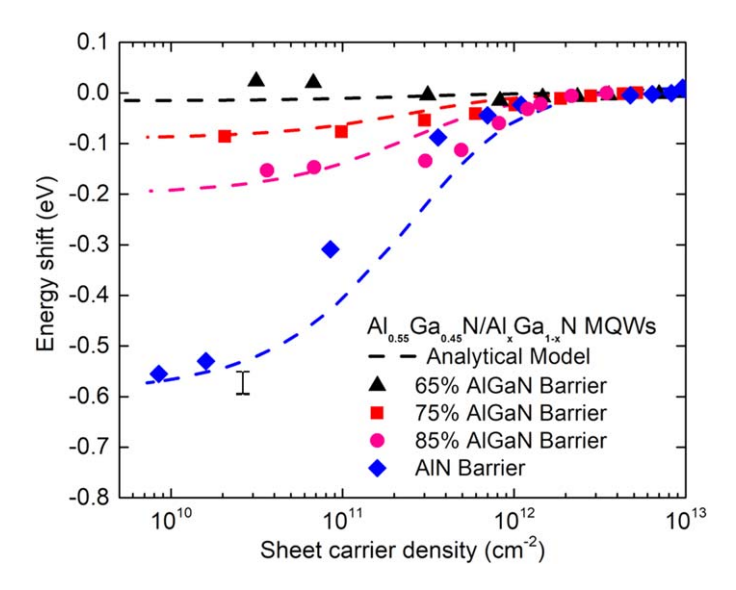


**Fig. 2.** (Color online) Relative energy shift of MQW emission for structures for fixed well and barrier widths but different Al contents in the barriers. Symbols correspond to the experimental data and dashed curves correspond to the energy shift calculated based on the analytical model in Eq. (1). For higher Al contents a stronger shift is observed, which is due to a stronger QCSE.

**Table I.** Electric field in MQW structures determined experimentally from power-dependent PL measurements. The error corresponds to the fit error and estimated well width variation.

Barrier composition	$Al_{0.65}Ga_{0.75}N$	$Al_{0.75}Ga_{0.25}N$	$Al_{0.85}Ga_{0.15}N$	AlN
Electric field (MV cm <sup>-1</sup> )	$0.5 \pm 0.4$	$1.2 \pm 0.3$	$1.8 \pm 0.3$	$2.8 \pm 0.6$

less pronounced. The fit of the experimental data using Eq. (1) and a screening coefficient of  $5 \times 10^{11}$  cm<sup>-2</sup> is displayed as dashed lines in Fig. 2. The fit is generally in good agreement between the analytical model and the experimental values and allows for extraction of the built-in electric field, which is summarized in Table I.

In order to analyze these results, we consider the origin of the built-in electric field in the AlGaN QW structures. The electric field is induced by the accumulation of polarization charges at the interface between the wells and barriers, taking into account both SP and PZ; since all AlGaN-based MQWs grown on AlN substrates are under compression, both SP and PZ have the same sign. <sup>15,16,18,21)</sup> In this case, the electric field for a single QW (SQW) can be written as the difference of the polarization in the barriers and wells, given by:

$$F_{\rm w} = (P_{\rm sp}^{\rm b} + P_{\rm pz}^{\rm b} - P_{\rm sp}^{\rm w} - P_{\rm pz}^{\rm w}) / \varepsilon_0 \varepsilon_{\rm w}$$
 (3)

where  $P_{\text{sp,pz}}^{\text{w}}$  ( $P_{\text{sp,pz}}^{\text{b}}$ ) is the SP and PZ of the well (barrier). In this case, the electric field does not depend on the well width, rather it is determined only by the polarization. In contrast, for MQWs, the width of the barriers and wells needs to be considered. In this case, the electric field can be evaluated from the periodic boundary condition:

$$F_{\rm w} = L_{\rm b}(P_{\rm sp}^{\rm b} + P_{\rm pz}^{\rm b} - P_{\rm sp}^{\rm w} - P_{\rm pz}^{\rm w}) / [\varepsilon_0(L_{\rm w}\varepsilon_{\rm b} + L_{\rm b}\varepsilon_{\rm w})] \qquad (4)$$

where  $L_{\rm b,w}$  are the widths of the barriers and wells. The value of the spontaneous polarization charge in AlGaN can be interpolated using Vegard's law considering GaN and AlN as end members. Bowing, though discussed in the literature, <sup>15)</sup> does not make a significant contribution and is not considered. The value for the piezoelectric polarization charge is calculated using the elastic and piezoelectric tensors. All the material parameters used in these estimations are taken from the literature. <sup>15,20)</sup>

Figure 3 compares the theoretical and experimental results of the electric field strength in AlGaN MQWs as a function of the Al content in the barriers. As expected, and in agreement with the experimental results, the electric field strength is on the order of MV cm<sup>-1</sup> and increases with increasing Al content in the barriers. The solid line is calculated by assuming the zinc-blende (ZB) reference structure and proper PZ,<sup>15)</sup> while the dashed line represents the hexagonal (H) reference structure with improper PZ.<sup>20)</sup> The experimental values from Table I are also plotted in the graph. The experimentally determined fields show a similar dependence. However, considering the error bars, which arise mainly from well and barrier width variation and fitting, it is not possible to assign the experimental values to a specific model calculation.

The electric field for MQWs with AlN barriers is estimated to be as high as  $2.8\,\mathrm{MV\,cm^{-1}}$  (Table I, Fig. 3). Since high electric fields lead to a strong QCSE, which reduces the IQE of MQWs, this result implies that AlGaN/AlGaN MQWs should be superior to AlGaN/AlN MQWs. However, for the design of the active region one needs to consider that a thin QW can also significantly reduce the spatial separation between the electrons and holes and improve the IQE. Reference 11 reported a high IQE of 95% at a carrier density of  $10^{18}\,\mathrm{cm^{-3}}$  in  $3\times\,\mathrm{Al_{0.55}Ga_{0.45}N/AlN}$  MQWs (2.5 nm/ 2.5 nm). In addition, the QCSE can be significantly reduced or even eliminated under high excitation powers, as shown in Fig. 2. The estimated carrier density under a pumping power of  $95\,\mathrm{kW\,cm^{-2}}$  is  $\sim 10^{19}\,\mathrm{cm^{-3}}$  (sheet carrier density of  $\sim 10^{12}\,\mathrm{cm^{-2}}$ ), which is found to be a typical threshold carrier density for III-nitride laser diodes.  $^{11,25,37}$ )

Since the built-in electric field also depends on the barrier thickness in the MQW structures (Eq. 4), Fig. 4 shows the PL spectra of four Al<sub>0.55</sub>Ga<sub>0.45</sub>N/AlN MQW samples with various barrier thicknesses of 0.5, 1, 2 and 4 nm; the black

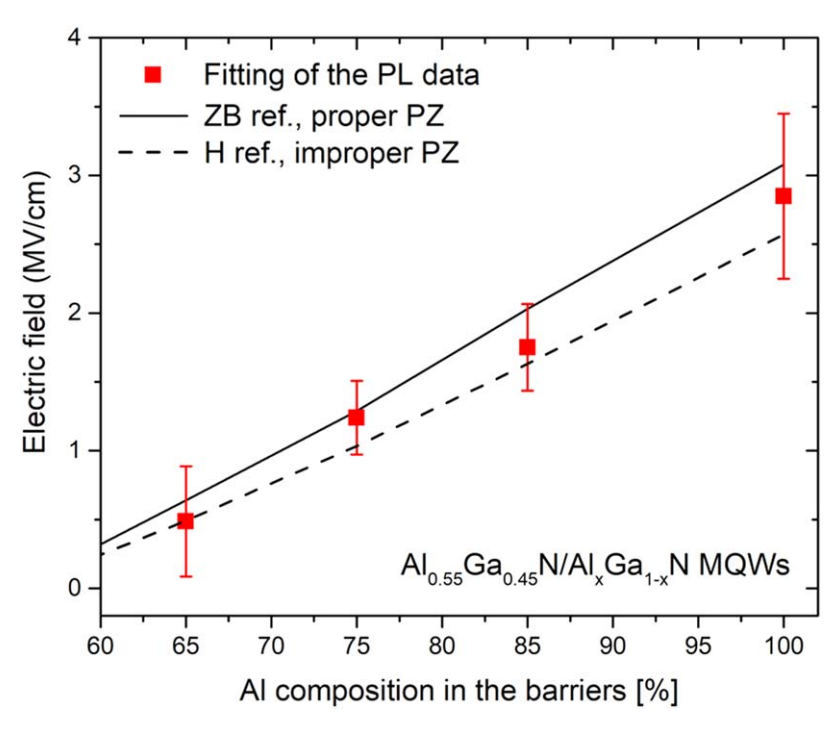


**Fig. 3.** (Color online) Built-in electric field strength in AlGaN MQW structures with an Al content of 55% in the wells as a function of the Al content in the barriers. Red squares are values deduced from the fitting of the PL data. The solid line is calculated by assuming the zinc-blende (ZB) reference structure and proper PZ, while the dashed line is representing the hexagonal reference (H) structure with improper PZ.

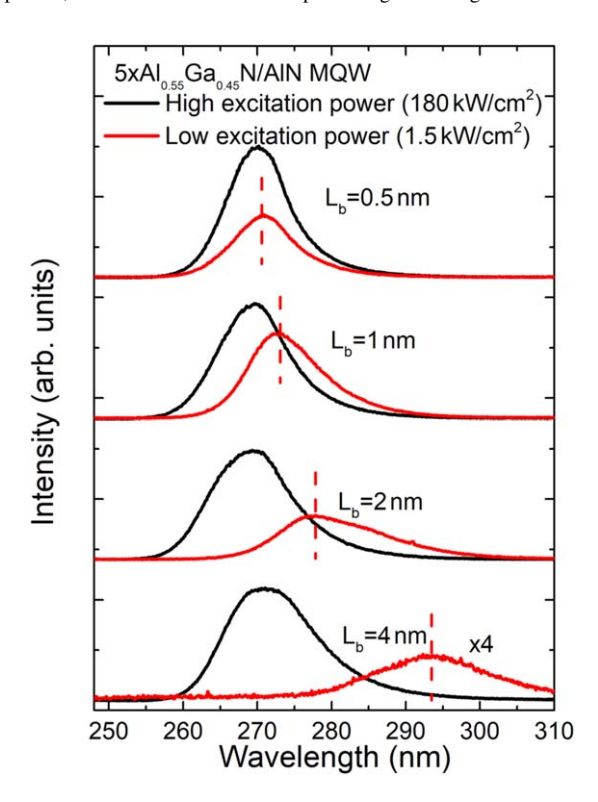


**Fig. 4.** (Color online) High  $(180 \text{ kW cm}^{-2})$  and low  $(1.5 \text{ kW cm}^{-2})$  excitation power PL data for AlGaN/AlN MQWs with barrier thicknesses of 0.5, 1, 2 or 4 nm at room temperature (297 K). Significant carrier screening is observed for high excitation power as indicated by a relatively constant PL peak position.

lines represent the PL spectra under a high excitation power density (180 kW cm<sup>-2</sup>), while the red lines show PL spectra taken under a low excitation power density (1.5 kW cm<sup>-2</sup>). For a high excitation power density, the peak position is around 270 nm and does not change with barrier thickness. This observation follows the previously described carrier

screening hypothesis. In contrast, when the excitation power density is sufficiently low, carrier screening is negligible. Based on Eq. 4, the electric field increases significantly for thicker AlN barriers, resulting in the observed red shift of the emission wavelength with increasing barrier thickness. These results, along with the aforementioned barrier composition study, show that the built-in electric field is a function of barrier strength, i.e. thickness and the Al composition of the barrier, which explains the discrepancy for polarization fields in AlGaN QWs in the literature. <sup>14,30,31)</sup>

Figure 5 shows the functional relationship between the barrier thickness and built-in electric field for AlN barriers. The red squares represent the experimentally determined electric fields for different barrier thicknesses using the same fitting procedure as in Table I. The electric field increases from 0.4 to 2.6 MV cm<sup>-1</sup> when the barrier thickness increases from 0.5 nm to 4 nm. The theoretical curve based on Eq. (4) is plotted as a solid line and is in good agreement with the experimental values. It is worth noting that when the barrier thickness approaches infinity, this limit will be described by the SQW condition and Eq. (3). The electric field in our Al<sub>0.55</sub>Ga<sub>0.45</sub>N/AlN SQW is predicted to be around 5 MV cm<sup>-1</sup>. This value is consistent with the theoretical calculation based on Eq. (3). These results show that, in combination with a thin well, the implementation of a thin AlGaN barrier can further reduce the impact of the QCSE. In addition, our previous results have found that a thin AlGaN barrier can significantly improve carrier injection in a UV laser diode. 11) Thus, in addition to thin wells, the use of thin AlGaN barriers is preferred in UV laser design, which is consistent with the underlying physics described above.

# 4. Conclusion

In summary, an analytical model was used to evaluate the electric field strength in AlGaN MQWs. The results showed

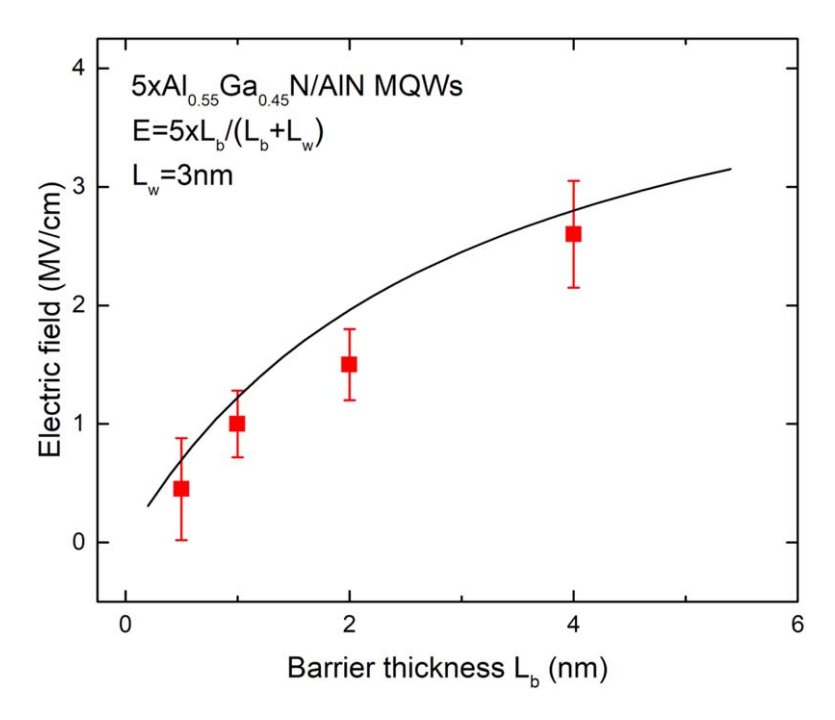


Fig. 5. (Color online) The dependence of the built-in electric field on AlN barrier width. The red squares are experimental results fitted to Eq. (1), while the black line corresponds to the electric field calculated from Eq. (4). Error bars correspond to the fitting error and possible variation of well width.

that a strong QCSE can be induced by greater barrier strength, i.e. a thicker barrier and/or more Al in the barrier. Electric fields as high as  $3\,\text{MV}\,\text{cm}^{-1}$  were observed in  $Al_{0.55}Ga_{0.45}N/AlN$  MQWs; an extrapolation of the barrier width to large values enabled us to estimate the electric field for an  $Al_{0.55}Ga_{0.45}N$  SQW as  $\sim 5\,\text{MV}\,\text{cm}^{-1}$ . These results provide crucial guidelines for design and optimization of AlGaN MQWs for UV emitters.

#### **Acknowledgments**

We acknowledge funding in part from NSF (ECCS-1508854, ECCS-1610992, DMR-1508191, ECCS-1653383), ARO (W911NF-15-2-0068, W911NF-16-C-0101 W911NF-18-1-0415, W911NF-14-C-0008), and AFOSR (FA9550-17-1-0225).

- 1) Y. Taniyasu, M. Kasu, and T. Makimoto, Nature 441, 325 (2006).
- T. Oto, R. G. Banal, K. Kataoka, M. Funato, and Y. Kawakami, Nat. Photonics 4, 767 (2010).
- 3) K. Balakrishnan, T. Katona, and A. Khan, Nat. Photonics 2, 77 (2008).
- Z. Bryan, I. Bryan, J. Xie, S. Mita, Z. Sitar, and R. Collazo, Appl. Phys. Lett. 106, 142107 (2015).
- I. Bryan, A. Rice, L. Hussey, Z. Bryan, M. Bobea, S. Mita, J. Xie, R. Kirste, R. Collazo, and Z. Sitar, Appl. Phys. Lett. 102, 61602 (2013).
- 6) J. Xie et al., Appl. Phys. Lett. 102, 171102 (2013).
- 7) X.-H. Li et al., Appl. Phys. Lett. 106, 41115 (2015).
- 8) R. Kirste, N. Rohrbaugh, I. Bryan, Z. Bryan, R. Collazo, and A. Ivanisevic, Annu. Rev. Anal. Chem. 8, 149 (2015).
- 9) Q. Guo, R. Kirste, P. Reddy, S. Mita, R. Collazo, and Z. Sitar, 2018 IEEE Res. Appl. Photonics Def. Conf. (IEEE, 2018), p. 131.
- K. Ban, J. Yamamoto, K. Takeda, K. Ide, M. Iwaya, T. Takeuchi, S. Kamiyama, I. Akasaki, and H. Amano, Appl. Phys. Express 4, 52101 (2011).
- R. Kirste, Q. Guo, J. H. Dycus, A. Franke, S. Mita, B. Sarkar, P. Reddy, J. M. LeBeau, R. Collazo, and Z. Sitar, Appl. Phys. Express 11, 82101 (2018).
- I. Bryan, Z. Bryan, M. Bobea, L. Hussey, R. Kirste, R. Collazo, and Z. Sitar, J. Appl. Phys. 116, 133517 (2014).
- R. G. Banal, Y. Taniyasu, and H. Yamamoto, Appl. Phys. Lett. 105, 053104 (2014).

- 14) S. Ichikawa, Y. Iwata, M. Funato, S. Nagata, and Y. Kawakami, Appl. Phys. Lett. 104, 252102 (2014).
- H. Morkoç, Handbook of Nitride Semiconductors and Devices Vol. 1: Materials Properties, Physics and Growth (Wiley, Weinheim, 2008).
- 16) N. Grandjean, B. Damilano, S. Dalmasso, M. Leroux, M. Laügt, and J. Massies, J. Appl. Phys. 86, 3714 (1999).
- F. Bernardini, V. Fiorentini, and D. Vanderbilt, Phys. Rev. B 56, R10024 (1997).
- 18) E. Kuokstis et al., Appl. Phys. Lett. 81, 4130 (2002).
- 19) S.-H. Park and S.-L. Chuang, Appl. Phys. Lett. 76, 1981 (2000).
- C. E. Dreyer, A. Janotti, C. G. Van de Walle, and D. Vanderbilt, Phys. Rev. X 6, 21038 (2016).
- A. Bonfiglio, M. Lomascolo, G. Traetta, R. Cingolani, A. Di Carlo, F. Della Sala, P. Lugli, A. Botchkarev, and H. Morkoc, J. Appl. Phys. 87, 2289 (2000).
- 22) T. Takeuchi, S. Sota, M. Katsuragawa, M. Komori, H. Takeuchi, H. Amano, and I. Akasaki, Jpn. J. Appl. Phys. 36, L382 (1997).
- M. Leroux, N. Grandjean, J. Massies, B. Gil, P. Lefebvre, and P. Bigenwald, Phys. Rev. B 60, 1496 (1999).
- 24) K. A. Bulashevich, S. Y. Karpov, and R. A. Suris, Phys. Status Solidi 243, 1625 (2006).
- H. Zhao, R. A. Arif, Y.-K. Ee, and N. Tansu, IEEE J. Quantum Electron. 45, 66 (2009).
- 26) M. Rychetsky et al., J. Appl. Phys. 119, 95713 (2016).
- C. Y. Lai, T. M. Hsu, W.-H. Chang, K.-U. Tseng, C.-M. Lee, C.-C. Chuo, and J.-I. Chyi, J. Appl. Phys. 91, 531 (2002).
- 28) T. M. Hsu, C. Y. Lai, W.-H. Chang, C.-C. Pan, C.-C. Chuo, and J.-I. Chyi, Appl. Phys. Lett. 84, 1114 (2004).
- 29) T. Takeuchi, C. Wetzel, S. Yamaguchi, H. Sakai, H. Amano, I. Akasaki, Y. Kaneko, S. Nakagawa, Y. Yamaoka, and N. Yamada, Appl. Phys. Lett. 73, 1691 (1998).
- 30) A. Pinos, S. Marcinkevičius, K. Liu, M. S. Shur, E. Kuokštis, G. Tamulaitis, R. Gaska, J. Yang, and W. Sun, Appl. Phys. Lett. 92, 61907 (2008).
- Z. A. Bryan, Ph.D. Thesis Faculty of Materials Science and Engineering, North Carolina State University, Raleigh (2015).
- 32) A. Rice, R. Collazo, J. Tweedie, R. Dalmau, S. Mita, J. Xie, and Z. Sitar, J. Appl. Phys. 108, 43510 (2010).
- 33) I. Bryan, C. R. Akouala, J. Tweedie, Z. Bryan, A. Rice, R. Kirste, R. Collazo, and Z. Sitar, Phys. Status Solidi Curr. Top. Solid State Phys. 11, 454 (2014).
- 34) R. Dalmau et al., J. Electrochem. Soc. 158, H530 (2011).
- Z. Bryan, I. Bryan, S. Mita, J. Tweedie, Z. Sitar, and R. R. Collazo, Appl. Phys. Lett. 106, 232101 (2015).
- 36) W. Guo et al., J. Appl. Phys. 115, 103108 (2014).
- H. Yoshida, M. Kuwabara, Y. Yamashita, K. Uchiyama, and H. Kan, Appl. Phys. Lett. 96, 211122 (2010).